Journal of Structural Biology xxx (2019) xxx-xxx

Contents lists available at ScienceDirect

Journal of Structural Biology

journal homepage: www.elsevier.com

NADPH-dependent sulfite reductase flavoprotein adopts an extended conformation unique to this diflavin reductase

Angela M. Tavolieri[a], Daniel T. Murray[a], Isabel Askenasy[a, 1], Joseph M. Pennington[a], Lauren McGarry[a], Christopher B. Stanley[b], M. Elizabeth Stroupe[a, *]

[a] Department of Biological Science and Institute of Molecular Biophysics, 91 Chieftain Way, Tallahassee, FL 32306, USA
[b] Neutron Scattering Division, Oak Ridge National Laboratory, P.O. Box 2008, MS 6743, Oak Ridge, TN 37831, USA

ARTICLE INFO

Keywords:
Flavoprotein
Diflavin reductase
Cytochrome p450 reductase
Electron transfer
X-ray crystallography
SANS

ABSTRACT

This is the first X-ray crystal structure of the monomeric form of sulfite reductase (SiR) flavoprotein (SiRFP-60) that shows the relationship between its major domains in an extended position not seen before in any homologous diflavin reductases. Small angle neutron scattering confirms this novel domain orientation also occurs in solution. Activity measurements of SiR and SiRFP variants allow us to propose a novel mechanism for electron transfer from the SiRFP reductase subunit to its oxidase metalloenzyme partner that, together, make up the SiR holoenzyme. Specifically, we propose that SiR performs its 6-electron reduction via intramolecular or intermolecular electron transfer. Our model explains both the significance of the stoichiometric mismatch between reductase and oxidase subunits in the holoenzyme and how SiR can handle such a large volume electron reduction reaction that is at the heart of the sulfur bio-geo cycle.

1. Introduction

Sulfur reduction is part of an ancient and essential bio-geo cycle that maintains electrochemical homeostasis across diverse biological niches (Barton et al., 2017; Huang et al., 2017; Singh and Lin, 2015; Wasmund et al., 2017). In proteobacteria, a heteromeric NADPH-dependent oxidoreductase, sulfite reductase (SiR), serves in the sulfur assimilation pathway to reduce sulfite (SO_3^{2-}) by six electrons, generating sulfide (S^{2-}) for incorporation into sulfur-containing biomolecules (Siegel et al., 1973). SiR has two subunits. The flavoprotein (SiRFP) is a cytochrome p450 reductase (CPR) homolog that binds NADPH, FAD, and FMN cofactors (Siegel and Davis, 1974). The hemoprotein (SiRHP) is an iron metalloenzyme that houses the active site (Siegel et al., 1973).

The analogy to CPR is useful in thinking about SiRFP structure and function because SiRFP and CPR have the same three domains (Fig. 1A). An N-terminal FMN-binding flavodoxin (Fld) domain is followed by a linker to a FAD and NADPH binding domain that is homologous to flavodoxin reductase (FNR), interrupted by a connection domain (Eschenbrenner et al., 1995a,b). CPR undergoes a redox-dependent two-state conformational change in which the Fld domain can be closed (oxidized) or open (reduced) relative to the connection/FNR domains, mediated by the hinge motion of an interdomain linker (Freeman et al., 2017; Hamdane et al., 2009; Wang et al., 1997; Xia et al., 2011). The closed conformation allows inter-flavin electron transfer whereas the open conformation allows close approach of the oxidase partner (Freeman et al., 2017, 2018; Hamdane et al., 2009; Huang et al., 2013; Laursen et al., 2011; Sugishima et al., 2014; Wang et al., 1997; Xia et al., 2011).

An internal truncation within the CPR linker constrains this domain movement and the resulting CPR variant functions if electrons are donated directly to the FMN but not if they are supplied as NADPH

Abbreviations: SiR, sulfite reductase; SiRFP, sulfite reductase flavoprotein; SiRHP, sulfite reductase hemoprotein; CPR, cytochrome p450 reductase; CYP, cytochrome p450; NOS, nitric oxide synthase; MSR, methionine synthase reductase; BM3, bacterial cytochrome p450 BM3; SPG, succinic acid, sodium dihydrogen phosphate and glycine buffer; SANS, small angle neutron scattering.

* Corresponding author.
Email address: mestroupe@bio.fsu.edu (M.Elizabeth Stroupe)
[1] Current address: Department of Biomolecular Chemistry, University of Wisconsin, School of Medicine and Public Health, 440 Henry Mall, Biochemical Sciences Building, Room 4206C, Madison, WI 53706, USA.

https://doi.org/10.1016/j.jsb.2019.01.001
Received 26 September 2018; Received in revised form 30 December 2018; Accepted 3 January 2019
Available online xxx
1047-8477/ © 2019.

UNCORRECTED PROOF

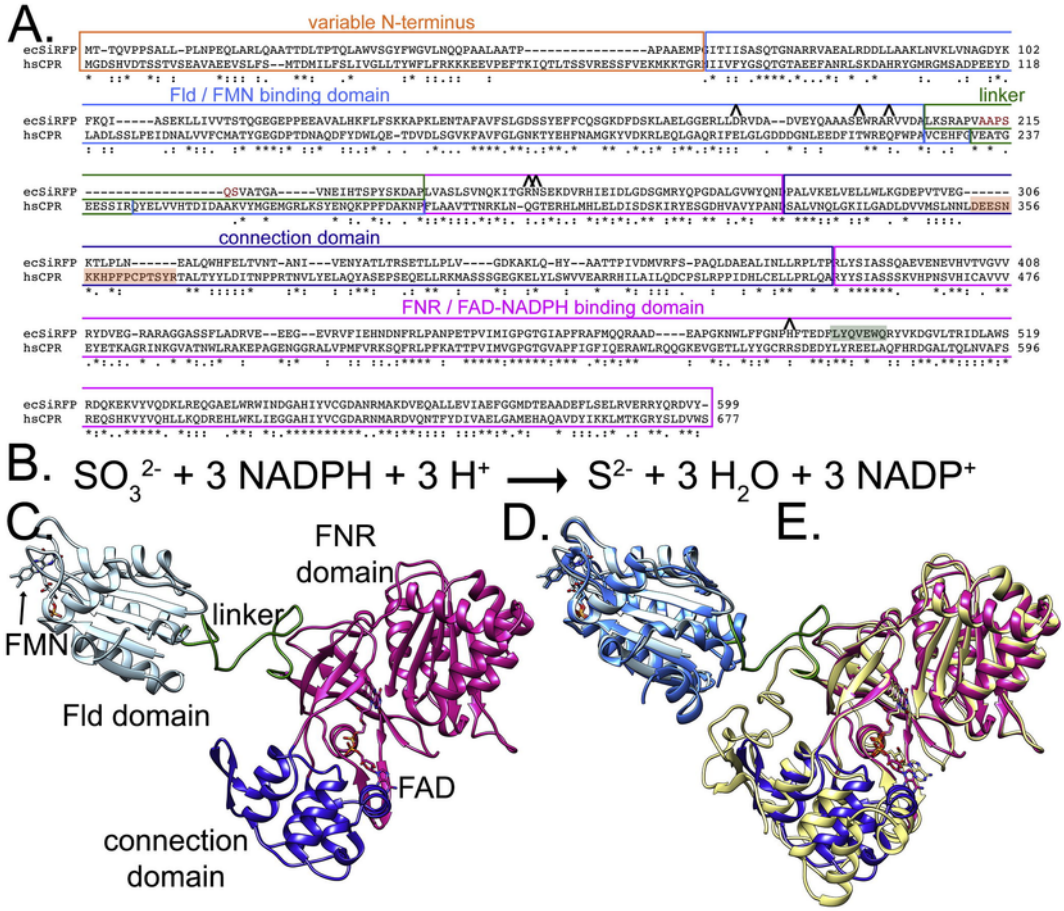

Fig. 1. Sequence homology between SiRFP and its CPR homolog is high. A. Pairwise alignment of the *E. coli* SiRFP sequence (ecSiRFP) and *Homo sapien* CPR (hsCPR). The domains are as follows: variable N-terminus (orange); Fld-like domain (light blue); flexible, inter-domain linker (green); FNR-like domain (violet); and the connection domain that interrupts the FNR domain (blue). A loop insertion in CPR's connection domain is highlighted in orange and the SiRHP binding site (FLYQVEW) is highlighted in green. B. The chemical reaction that assimilatory, NADPH-dependent SiR performs. C. The overall, extended structure of SiRFP-60-ΔAAPSQS with the domains, minus the N-terminus, colored as in A. D. Superimposition of SiRFP-60's Fld domain with hsCPR (bright blue, PDB ID 3QE2 (Xia et al., 2011)). E. Superimposition of SiRFP-60's connection/FNR domains with hsCPR (yellow, PDB ID 3QE2 (Xia et al., 2011)).

(Hamdane et al., 2009). The effect of an analogous truncation on oligomeric SiR was untested until this study. CPR homologs like the nitric oxide synthase reductase module (NOS_{red}), eukaryotic methionine synthase reductase (MSR), and bacterial cytochrome p450 BM3 reductase module ($BM3_{red}$) also function through a similar conformational change, albeit with isoform-specific conformational switching rates (Haque et al., 2014; Yokom et al., 2014; Zhang et al., 2018). How SiRFP fits into this paradigm has also not been formally tested until now.

Three properties set SiRFP apart from CPR, NOS_{red}, MSR, and $BM3_{red}$ beyond its high-volume electron transfer that requires consumption of three NADPH equivalents per turnover event (Fig. 1B). First, when expressed as the full-length protein, SiRFP is an octamer whose oligomerization is mediated by its first 52 amino acids (Siegel and Davis, 1974; Siegel et al., 1973; Zeghouf et al., 2000), Fig. 1A). The protein is a monomer if expressed as a 60 kDa N-terminal truncation (SiRFP-60, (Zeghouf et al., 1998)). In contrast, CPR is a monomer that is anchored to membrane by N-terminal hydrophobic amino acids (Kasper, 1971). Second, the linker between the Fld and FNR domains in SiRFP is considerably longer (30 amino acids) than in CPR (12 amino acids) (Fig. 1A). Third, SiRFP binds tightly to SiRHP (Askenasy et al., 2018; Siegel et al., 1973; Zeghouf et al., 2000). The octamer binds 4 copies of SiRHP (Askenasy et al., 2015; Siegel and Davis, 1974) but SiRHP is a monomer if expressed alone (Smith and Stroupe, 2012; Wu et al., 1991). In contrast, CPR binds transiently in a 1:1 fashion with various cytochrome oxidase partners (Im and Waskell, 2011). NOS and BM3 are oxidase-reductase gene-fusion products in which electron transfer is governed by a transient interaction across subunits, between a reductase domain from one subunit and the oxidase domain of another (Haque et al., 2012; Panda et al., 2001, 2002; Siddhanta et al., 1996, 1998; Zhang et al., 2018). Methionine synthase (MS) is a dimer that forms a tetramer with two MSR subunits that form a dynamic oxidoreductase (Olteanu and Banerjee, 2001; Olteanu et al., 2004; Wolthers and Scrutton, 2007; Wolthers et al., 2003, 2007).

The evolutionary advantage stemming from SiR's subunit stoichiometric mismatch is not well understood. Ancestral sulfite reductases that allow sulfate reducing organisms to use sulfite as the terminal electron acceptors in anaerobic respiration, called dissimilatory sulfite reductases (DSRs), were either homodimers or heterodimers (Crane and Getzoff, 1996). One hypothesis proposes that the mismatch recalls a time when there were two, not one, SiRHP active sites for each globular unit (Crane and Getzoff, 1996). This hypothesis falls apart, however, because DSRs can use either transiently interacting ferredoxin reductase partners or a fused ferredoxin-like domain as their reductase partners (Hsieh et al., 2010; Oliveira et al., 2008; Parey et al., 2010; Schiffer et al., 2008). DSR also differs from SiR because dissimilatory homologs release partially-reduced thiosulfate ($S_2O_3^{2-}$), an environmental pollutant (Hsieh et al., 2010). We recently showed that SiRHP binds SiRFP at a position within the FNR domain that is far from where electrons are transferred from the Fld domain (Askenasy et al., 2018,

Table 1
Data collection and refinement statistics.

	SiRFP-60-ΔAAPSQS
Data collection	
Space group	P 2(1) 2(1) 2(1)
Cell dimensions	
a, *b*, *c* (Å)	60.5, 99.7, 103.5
α,β,γ (°)	90, 90, 90
Resolution (Å)	45.95–2.34 (2.42–2.34)
R_{pim}	0.034 (0.099)
$I/\sigma I$	23.94 (8.72)
Completeness (%)	99.7 (97.45)
Redundancy	7.3 (6.6)
Refinement	
Resolution (Å)	45.9–2.34 (2.38–2.34)
No. reflections	26,979 (2595)
R_{work}	0.168 (0.174)
R_{free}	0.234 (0.266)
No. atoms	4728
Protein	4230
Ligand/ion	144
Water	354
B-factors (Å^2)	
Protein	38.0
Ligand/ion	44.4
Water	33.7
R.m.s. deviations	
Bond lengths (Å)	0.007
Bond angles (°)	0.886

2015), which led to a new hypothesis: a structural interaction forms between SiRFP's FNR domain and a tightly bound SiRHP whereas a functional interaction forms between SiRFP's Fld domain and a transiently interacting SiRHP.

Environmental SO_3^{2-} hinders bioremediation efforts of other toxins by sulfate reducing bacteria (Townsend et al., 1997). A recently-reported synthetic sulfite reductase built into a cytochrome p450 (CYP) scaffold mimics DSR's incomplete conversion of SO_3^{2-} to S^{2-} (Mirts et al., 2018), an exciting development in the effort to make a designed protein catalyst that reduces SO_3^{2-} to enhance the potential for bioremediation by sulfate reducing bacteria. Designing an enzyme that captures SiR's ability to completely convert SO_3^{2-} to S^{2-} is the next challenge, aided by a fuller understanding of the mechanistic details underlying SiR's electron transfer.

Here, we present the first X-ray crystal structure of SiRFP-60 to show all three of its domains in a single structure. SiRFP-60's Fld domain takes an extremely extended position relative to the FNR domain when trapped through the internal linker deletion of amino acids 212–217 (SiRFP-60-ΔAAPSQS). Even without the internal truncation, SiRFP-60 adopts this extended orientation in solution, measured by small angle neutron scattering (SANS). Interestingly, crystal packing of SiRFP-60-ΔAAPSQS simultaneously mimics the closed conformation where a Fld domain comes from a nearby symmetry partner. Another Fld domain from a symmetry-derived subunit interacts with the FNR domain, positioning the FMN cofactor towards the SiRHP binding site. We analyzed the ability of NADPH or sodium dithionite to reduce four variants of SiRFP (octameric wild-type, octameric ΔAAPSQS, SiRFP-60, and SiRFP-60-ΔAAPSQS). Each variant was reduced by either reductant but the ΔAAPSQS deletion inhibits SiRFP-60's ability to reduce SiRHP in the heterodimer or a cytochrome *c* partner. The ΔAAPSQS deletion has no impact on the function of the SiR holoenzyme. Together, these observations support the hypothesis that the long linker joining the Fld and FNR domains is essential for intramolecular electron transfer and electron transfer to either a tightly-bound SiRHP (in *cis*) or to a SiRHP bound to an adjacent SiRFP (in *trans*). This new understanding has broad implications in explaining the stoichiometric mismatch between the SiRFP and SiRHP subunit number in the holoenzyme because SiR needs six electrons that come from 3 independent NADPH molecules to complete the chemical transformation of sulfite into sulfide.

2. Materials and methods

Protein expression and purification: Escherichia coli cells were transformed with a pBAD plasmid harboring the *cysJ* gene but with a 5′ deletion (nucleotides 1–156, corresponding to amino acids 1–52) for SiRFP-60 expression and, for SiRFP-60-ΔAAPSQS expression, an additional internal truncation of nucleotides 636–654, corresponding to amino acids 212–217. Cells expressing either SiRFP variant as N-terminal six-histidine fusions were grown in six liters of lysogeny broth supplemented with ampicillin and induced with 0.05% L-arabinose. Following growth and induction of protein expression, cells were harvested by centrifugation and resuspended in 10 mL of 1X succinic acid, sodium dihydrogen phosphate, and glycine buffer (SPG), pH 6.8, and 200 mM NaCl supplemented with one EDTA-free UltraCruz protease tablet (Santa Cruz Biotechnology, Dallas, TX USA) before cells were lysed via micro-fluidizer (Microfluidics, Westwood, MA, USA). Lysate was clarified by centrifugation at 16,000 × *g* for 30 min, after which 10% polyethyleneimine (PEI) was added, with 30 min stirring, at 4 °C. The PEI-containing mixture was then centrifuged at 10,000 × *g* for 30 min. The sample was injected onto a Ni-NTA column (GE Healthcare, Little Chalfont, United Kingdom) using an AKTA FPLC (GE Healthcare). SiRFP-60/SiRFP-60-ΔAAPSQS containing fractions were collected and loaded onto an anion exchange HiTrap-Q column (GE Healthcare). SiRFP-60/SiRFP-60-ΔAAPSQS containing fractions were concentrated in a 10,000 MWCO Spin-X centrifugal concentrator

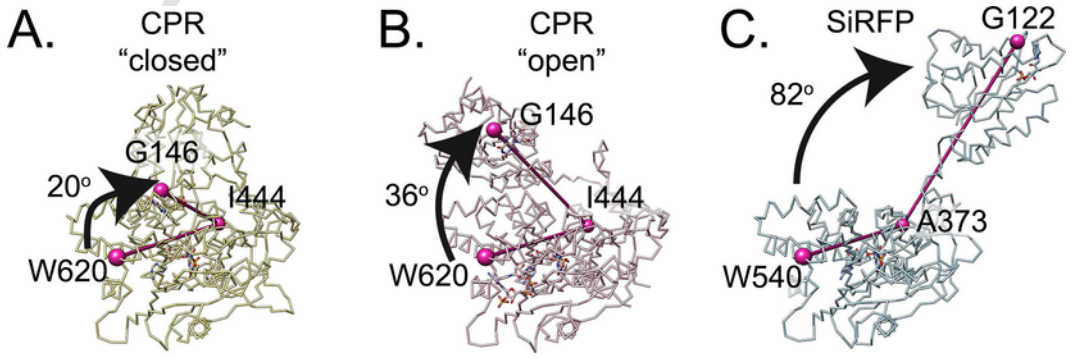

Fig. 2. SiRFP-60-ΔAAPSQS is in an extended conformation. A. In the closed CPR (PDB ID 3QE2 (Xia et al., 2011)), the N-terminal Fld domain, containing G146, is oriented to the connection/FNR domains, containing I444 (connection domain) and W620 (FNR domain) at a 20° angle. B. In the open CPR (PDB ID 3ES9 (Hamdane et al., 2009)), the N-terminal Fld domain is oriented to the connection/FNR domains at a 36° angle. C. In SiRFP-60-ΔAAPSQS, the N-terminal Fld domain, containing G122, is oriented to the connection/FNR domains, containing A373 (connection domain) and W540 (FNR domain) at an 82° angle.

CORRECTED PROOF

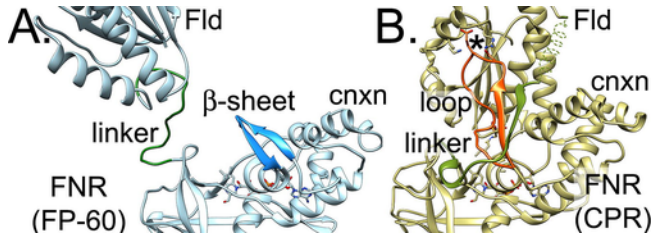

Fig. 3. SiRFP-60-ΔAAPSQS's Fld domain is nearly independent from the connection/FNR domains. A. A linker with no defined secondary structure (green) joins the two independent domains. A two-stranded β-sheet (bright blue) that is peripheral to the connection domain points to, but does not interact with, the Fld domain. B. In the closed conformation of CPR, the equivalent region to the two-stranded β-sheet in A (orange) is longer and does not form a perfect sheet. The loop forms salt bridges (*) with the Fld domain. The linker between the Fld and connection/FNR domains (olive green) is partially disordered (olive green dotted spring).

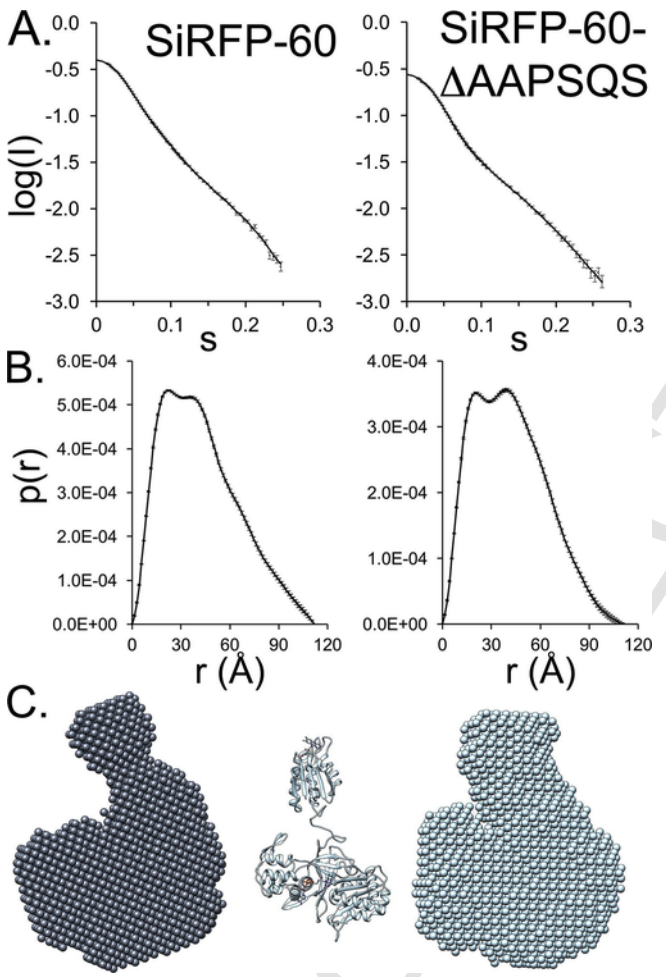

Fig. 4. SANS measurements support that SiRFP-60 and SiRFP-60-ΔAAPSQS are in an extended conformation in solution. A. Scattering curves of SiRFP-60 (left) and SiRFP-60-ΔAAPSQS (right) show gradual decay over scattering angle. B. Both SiRFP-60 (left) and SiRFP-60-ΔAAPSQS (right) show distance distributions consistent with extended molecules. C. Envelopes calculated from the scattering functions in A show extended shapes consistent with the extended asymmetric unit: SiRFP-60 envelope function (gray, left); SiRFP-60-ΔAAPSQS atomic model (middle); and SiRFP-60-ΔAAPSQS envelope function (light blue, right).

(Corning, Corning, NY, USA) at 4000 × *g* before being injected onto a HiPrep 26/60 Sephacryl S100-HR column (GE Healthcare). SiRFP-60/SiRFP-60-ΔAAPSQS containing fractions were concentrated with a 10,000 MWCO concentrator (Corning) at 5000 × *g* until the sample was

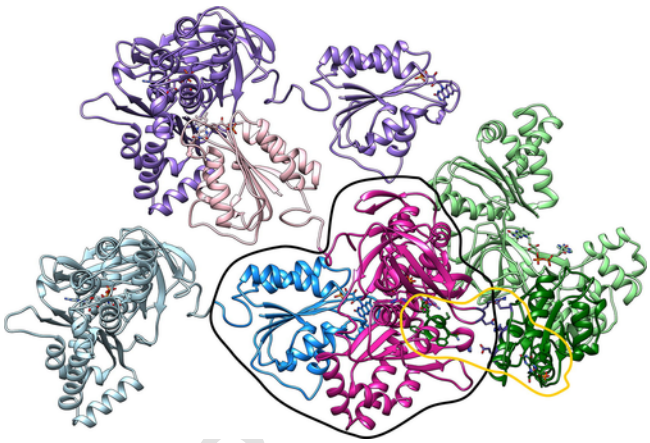

Fig. 5. Crystal contacts in the $P2_12_12_1$ SiRFP-60-ΔAAPSQS crystal. The central SiRFP-60-ΔAAPSQS molecule (Fld domain, light pink; connection/FNR domains, dark pink; and SiRHP binding site, green) interacts with a symmetry partner (bright/light blue) to replicate the closed conformation (circled in black), bringing the FMN cofactor from molecule 2 (dark blue) in close contact to the FAD cofactor from molecule 1 (dark pink). A third Fld domain (dark green) places the FMN cofactor within 20 Å of the SiRHP binding site (circled in gold). The amino acids that mediate this symmetry interaction are in purple, across the subunit-subunit interface of the molecules colored dark pink and dark green.

at 20 mg/mL. SiR, SiR-ΔAAPSQS, and SiRHP were expressed and purified as previously described (Askenasy et al., 2015).

Crystallization, X-ray diffraction, and refinement: SiRFP-60-ΔAAPSQS was subjected to a sparse matrix crystallization screen. An initial condition, 2 M ammonium sulfate, 100 mM N-cyclohexyl-3-aminopropane sulfonic acid (CAPS) at a pH of 10.5, and 200 mM lithium sulfate, was identified (Wizard screen, Rigaku, Bainbridge Island, WA, USA). In each drop, 1.2 μL of 20 mg/mL protein was added to 1.2 μL of precipitant. To obtain single, large protein crystals, smaller crystals were crushed and used to micro-seed in 1.8 M ammonium sulfate 0.1 M lithium sulfate and 0.1 M CAPS pH 10.5. Single crystals were frozen and shipped to SER-CAT beamline 22-BM at Argonne National Laboratory. Diffraction was collected on a MARMOSAIC-225 CCD detector (Rayonix, Evanston, IL USA) with a 1.0 Å wavelength beam from 46 to 2.3 Å resolution at 100 K. Initial phases were calculated with molecular replacement against the X-ray structure of the FNR domain (PDB ID 1DDG (Gruez et al., 2000)) with PHASER, implemented in Phenix (Adams et al., 2010) and the Fld domain (PDB ID 1YKG (Sibille et al., 2005)) was rigid-body fit into its corresponding density in Chimera (Pettersen et al., 2004). The structure was refined by phenix.refine using iterations of manual fitting and energy minimization in Coot (Emsley et al., 2010) and Phenix (Adams et al., 2010) resulting in a structure with 95.53% of the residues falling in the preferred region of the Ramachandran plot; 3.50% falling in allowed regions, and 0.97% as outliers.

Small-angle neutron scattering: SANS experiments were performed on the extended Q-range small-angle neutron scattering (EQ-SANS, BL-6) beam line at the Spallation Neutron Source (SNS) located at Oak Ridge National Laboratory (ORNL). In 60 Hz operation mode, two configurations were used: 4 m sample-to-detector distance with 2.5–6.1 Å wavelength band and 1.3 m sample-to-detector distance with 4.0–7.7 Å wavelength band (Zhao et al., 2010) to obtain the relevant wave-vector transfer, $Q = 4\pi \sin(\theta)/\lambda$, where 2θ is the scattering angle. Samples were loaded into 1 mm pathlength circular-shaped quartz cuvettes (Hellma USA, Plainville, NY) and SANS measurements performed at 8 °C. Data reduction followed standard procedures using MantidPlot (Arnold et al., 2014). The measured scattering intensity was corrected for the detector sensitivity and scattering contribution from the solvent and empty cells, and then placed on absolute scale using a calibrated standard (Wignell and Bates, 1987).

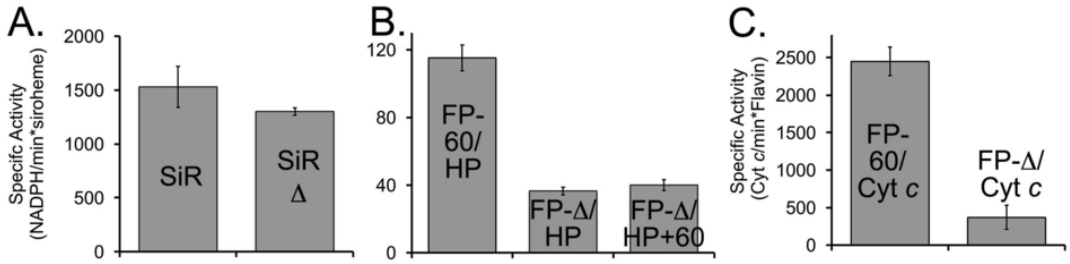

Fig. 6. Specific activities measurements. A. SiR holoenzyme with or without the ΔAAPSQS truncation and B. SiRFP-60/SiRHP dimer with or without the ΔAAPSQS deletion and free SiRFP-60. C. SiRFP-60 with or without the ΔAAPSQS deletion and cytochrome *c*.

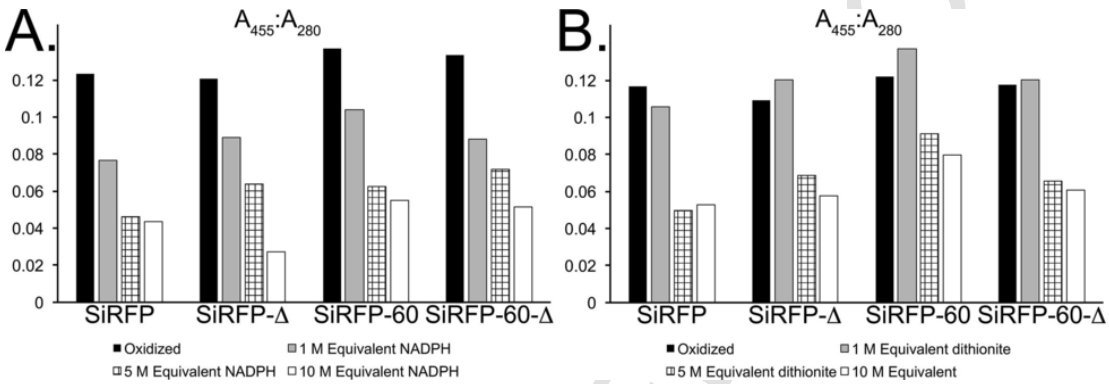

Fig. 7. Flavin cofactor reductions in SiRFP. A. NADPH and B. sodium dithionite reduction of SiRFP with or without the ΔAAPSQS truncation and SiRFP-60 with or without the ΔAAPSQS deletion at 1, 5, and 10 M equivalent reductant.

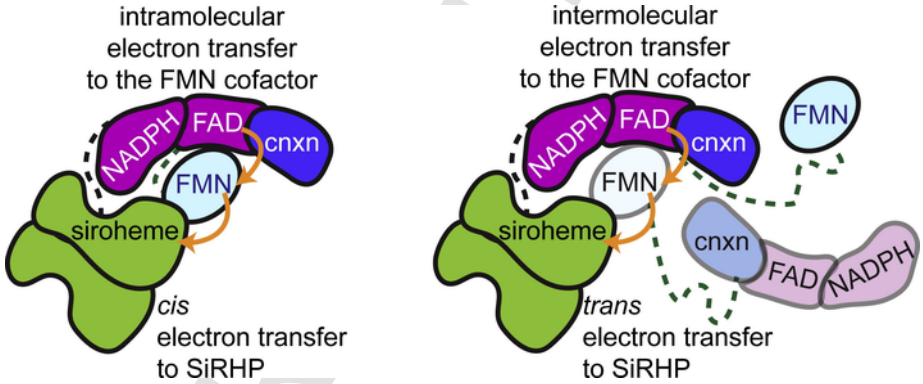

Fig. 8. Model for FAD to FMN electron transfer. We propose a model in which it can occur within a single SiRFP molecule (intra molecular) or across adjacent molecules (inter molecular) and then to a tightly-bound SiRHP (in *cis*) or to a SiRHP bound to an adjacent SiRFP (in *trans*).

Reduced data were imported into the ATSAS suite, managed in PRIMUS (Konarev et al., 2003; Petoukhov et al., 2012). R_g, D_{max}, and the distance distribution functions were calculated in GNOM (Svergun, 1992). Ten *ab initio* models were calculated and averaged to model the envelope function in DAMMIN (Svergun, 1999). Theoretical scattering curves of SiRFP-60-ΔAAPSQS and the open/closed conformations of CPR were calculated in CRYSON (Svergun et al., 1998).

Activity assays: We measured the specific activity of electron transfer from SiRFP to SiRHP either in the purified dodecameric SiR holoenzyme with wild-type SiRFP or SiRFP-ΔAAPSQS, or by mixing the SiRFP-60 variants and SiRHP at a 2:1 ratio. Activity was monitored spectrophotometrically at 340 nm to measure SO_3^{2-}-dependent NADPH oxidation. Reactions contained 1 mM potassium phosphate pH 7.7, 0.2 mM NADPH (Sigma-Aldrich, St. Louis, MO, USA), 10 units of glucose oxidase (Sigma-Aldrich, St. Louis, MO, USA), and 10 mM glucose, prepared in an anaerobic glove box (UNIlab, mBRAUN, Stratham, NH) and were initiated by injection of 5 μL of the enzyme to anaerobic cuvettes. Spectroscopic measurements were made on a 8454 UV–Vis diode array instrument (Agilent, Santa Clara, CA, USA).

Reduction of cytochrome *c* by SiRFP-60 or SiRFP-60-ΔAAPSQS was followed spectrophotometrically at 550 nm ($\varepsilon = 28\,mM^{-1}\,cm^{-1}$). The 1 mL reaction mixture was prepared anaerobically and contained 0.2 mM NADPH (Sigma-Aldrich, St. Louis, MO, USA), 0.05 mM oxidized cytochrome *c* from equine heart (Sigma-Aldrich), 10 units of glucose oxidase (Sigma-Aldrich), and 10 mM glucose in 50 mM Tris pH 7.5 buffer. The reactions were initiated by injection of 5 μL of 2.4 nM SiRFP-60 or SiRFP-60-ΔAAPSQS.

All enzymatic activities were background corrected for non-specific activity due to oxygen introduced during protein injection in a control reaction that did not include SO_3^{2-} in the SiRHP experiments or NADPH in the cytochrome *c* experiments.

Reduction assays: We measured the ability of NADPH or sodium dithionite to reduce SiRFP, SiRFP-ΔAAPSQS, SiRFP-60, or SiRFP-60-ΔAAPSQS by monitoring the absorbance at 458 nm. 0, 1, 5, or 10 M equivalents of each reductant was prepared in an anaerobic glove box

(UNIlab, mBRAUN) and incubated on ice for 30 min with 15 μM SiRFP variant that was previously passed over an anaerobically-equilibrated desalting column. All solutions were degassed using freeze-pumpthaw cycling and substitution by inert gas. Then, the solution was concentrated in a 30 kDa cutoff concentration device to harvest buffer to use as a spectroscopic blank that contained the same concentration of reductant. Samples and blanks were transferred to septa-sealed cuvettes and spectra were recorded on an 8454 spectrophotometer (Agilent).

Data and software availability: Coordinates and supporting experimental data were deposited in the Protein Data Bank under the accession ID 6EFV.

3. Results

3.1. Overall structure

SiRFP is modular like its homologs CPR, NOS_{red}, MSR, and $BM3_{red}$ (Fig. 1A). Unlike those monomeric or dimeric diflavin reductases, however, full length SiRFP is an octamer that can be made monomeric by removing the first 52 amino acids (Zeghouf et al., 1998). Even with this simplification, previous structure determination of SiRFP-60 failed to show the structural relationship between the domains because the extreme mobility of the Fld domain relative to the FNR domain left its density unresolved in the final model (Gruez et al., 2000). To overcome this limitation, we further synthesized an internal deletion of amino acids 212–217 (SiRFP-60-ΔAAPSQS) that enabled us to resolve both SiRFP domains in a single structure (Fig. 1C) that we refined to a resolution of 2.3 Å (Table 1).

As expected, both the N-terminal Fld domain and the C-terminal connection/FNR domains are highly similar to the prototypical diflavin reductase CPR. The Fld domain superimposes with an RMSD of 2.5 Å across all 144 atom pairs that are shared between SiRFP and human CPR (Fig. 1D). The connection/FNR domains superimpose with an RMSD of 4.4 Å across all 380 atom pairs that comprise that region (Fig. 1E). The two structures differ in the position of the connection domain, which is rotated towards the FAD cofactor and is far from the inter-subunit linker in SiRFP-60-ΔAAPSQS (Fig. 1E). The tightly-bound FMN and FAD cofactors bind as expected, with their isoalloxazine rings stacked against conserved hydrophobic amino acids (V188/Y158/F161 for FMN and Y388/Y599 for FAD) and their negative charged phosphate groups making ionic and hydrogen bonds with positively charged or polar amino acids (T72, D187, and Y388 for FMN and T332, R386, and S422 for FAD) (Fig. S1). The structure was determined without added NADPH but the pre-formed binding site remains virtually unchanged from the $NADP^+$-bound form seen in multiple CPR structures. The C-terminus of SiRFP is one amino acid shorter than CPR (Figs. 1A and S1), lacking the terminal serine that has been implicated in establishing the equilibrium of closed to open CPR conformations (Freeman et al., 2017; Hubbard et al., 2001).

3.2. SiRFP-60 is an extended reductase

Despite the shared folds of the individual domains, SiRFP-60-ΔAAPSQS adopts an extended conformation compared to oxidized (closed) or reduced (open) CPR. The relative orientation of the domains can be described by measuring the angle between two vectors, one drawn through the Fld domain connecting G146 to I444 (human CPR numbering) and the other drawn through the connection/FNR domains connecting I444 to W620. In the closed CPR conformation, the domains sit at a 20° angle relative to one another (Fig. 2A (Xia et al., 2011)). In the open CPR conformation, the domains are more extended and sit at a 36° angle relative to one another (Fig. 2B (Hamdane et al., 2009)). In SiRFP-60-ΔAAPSQS, the domains are nearly independent, sitting at an 82° angle relative to one another, in this case defined by connecting the homologous amino acids G122 to A373 and A373 to W540 (Fig. 2C). In this extended conformation, SiRFP's Fld domain projects away from the connection domain (Figs. 1C and 2C) in a distinct position from another extended CPR molecule, a yeast-human hybrid whose linker wraps around the connection domain to position the Fld domain towards the FNR domain (Fig. S2A (Aigrain et al., 2009)). In the original crystal structure of SiRFP-60, which only resolved the connection/FNR domains, there is a large channel where the Fld domain was present but disordered (Gruez et al., 2000). The Fld domain of SiRFP-60-ΔAAPSQS projects into the channel when the connection/FNR domains are superimposed (Fig. S2B). This extreme position of the Fld domain would not be possible in CPR because CPR's linker is only 12 amino acids long, compared to 24 amino acids in SiRFP-60-ΔAAPSQS (30 amino acids in SiRFP without the internal truncation).

3.3. The Fld domain is essentially free from its FNR domain

In addition to the additional amino acids present in the linker that connects the Fld and FNR domains (Fig. 1A), that stretch of protein is predicted to share characteristics associated with internal intrinsically disordered peptides (Askenasy et al., 2018). As expected, the 24 amino acid stretch in the ΔAAPSQS truncation does not adopt defined secondary structure, suggesting the linker does not rigidly constrain the domains with few, if any, interactions between the Fld domain and the connection/FNR domains (Fig. 1C). The independence of the Fld and connection/FNR domains in SiRFP-60-ΔAAPSQS arises from one of the major differences in the overall folds of SiRFP and CPR. In SiRFP, a two-stranded, anti-parallel beta sheet joined by a tight turn sits at the periphery of the connection domain that interrupts the FNR domain (Fig. 3). The solvent-exposed beta sheet is only four amino acids long and sits above the six short alpha helices that make up the body of the connection domain. In CPR, the analogous structural element is five amino acids long and an eight amino acid long loop links the two strands (Figs. 1A and 3). The loop connecting the beta strands is important for determining whether or not CPR is closed or open because salt bridges between loop amino acids and Fld domain amino acids in the closed conformation are broken when the Fld domain opens, governed by the reduction state of the FMN (Huang et al., 2013). Additionally, in CPR the linker between the domains acts as a third strand, wrapping around the connection domain to maintain contact between the Fld domain and the connection domain even in the open conformation. No such contacts exist in the extended conformation of SiRFP-60-ΔAAPSQS and the Fld domain is essentially free from the connection/FNR domains derived from the same polypeptide, projecting the FMN cofactor away from the FAD binding pocket.

3.4. SiRFP-60 is significantly more extended than CPR in solution

We wanted to assess whether the extended structure found in the crystal also occurred in solution and to test if it was a consequence of the internal ΔAAPSQS truncation. Therefore, we measured small-angle neutron scattering (SANS) from SiRFP-60 and SiRFP-60-ΔAAPSQS. From the one-dimensional scattering curves, we calculated a radius of gyration (R_g) for SiRFP-60 of 34.2 ± 0.4 Å (D_{max} of 113 Å) and an R_g for SiRFP-60-ΔAAPSQS of 33.2 ± 0.3 Å (D_{max} of 112 Å) (Fig. 4A and B). We next calculated the envelope function of SiRFP-60 and SiRFP-60-ΔAAPSQS from their one-dimensional scattering curves. The resulting envelopes derived from either SiRFP-60 variant compares well with the conformation seen in the X-ray crystal structure (Fig. 4C).

To compare these results with what we know about conformational variability of CPR, we calculated a series of theoretical scattering curves and R_gs from crystal structures of different conformations. Scattering curves calculated from crystal structures of either the open or closed CPR structure do not agree with the experimental data we mea-

UNCORRECTED PROOF

sured on SiRFP-60-ΔAAPSQS (Fig. S3A). The R_g calculated from CPR's open position is 25 Å and the R_g calculated from the closed conformation is 24 Å (Fig. S3B and C), close to SANS measurements made on CPR (Freeman et al., 2017). In contrast, a theoretical scattering curve calculated from our crystal structure compares well with our experimental SANS measurements (Fig. S3A). The theoretical R_g calculated from our crystal structure is 32 Å, also similar to those determined from the experimental scattering measurements (Figs. 4 and S3D). Taken together, the SANS data shows that SiRFP-60 with or without the internal linker deletion exists in solution in a significantly more extended conformation than its CPR counterpart.

3.5. A single connection-FNR domain is associated with two other Fld domains via symmetry contacts

One of the three symmetry partners generated by applying $P2_12_12_1$ symmetry projects its Fld domain into the central cavity between the connection and FNR domains in a similar position to the closed position seen in some crystal forms of CPR (Figs. 2A, 5, and S4A). As in CPR, the two domains in this mock-closed conformation sit at an angle of 20° relative to one another. SiRFP-60-ΔAAPSQS buries 850 $Å^2$ whereas CPR buries about half that surface area, 420 $Å^2$. In this way, both an open and closed conformation exist in the same crystal structure. An extensive array of well-ordered water-mediated hydrogen bonds between backbone amides and carbonyls also line the interface (Fig. S4B). Additionally, three salt bridges are important in maintaining this interaction (Fig. S4C). On one side of the Fld domain, pairing of D155 and R381 holds it to the connection domain. On the other side, salt bridges pair E121 with K560 and E126 with R596, holding the Fld domain to the FNR domain. These interactions are not conserved with CPR and are significantly different than the interactions that hold CPR in a closed conformation (Fig. S4B, C, and D). In this position, C7 from the FMN cofactor is about 4.4 Å away from C8 of the FAD cofactor (Fig. S1A), suggesting that although this alignment is not optimal for electron transfer, subtle changes to the positioning of the water-mediated interface, perhaps upon NADPH binding, could align the cofactors for productive electron transfer whether the Fld domain comes from the same polypeptide or an adjacent molecule in octameric, full length SiRFP.

A second symmetry partner from the $P2_12_12_1$ operation also interacts with the central connection/FNR domains, held by a salt bridge between D182 and R250, a hydrogen bond linking R200 to N251, and a water-mediated hydrogen bind between E196 to H491 and, and extensive water-mediated side-chain to backbone hydrogen bonds (Figs. 5 and S5). These amino acids are found in non-conserved regions of the protein (Fig. 1A). The FMN cofactor from this symmetry partner points towards the FNR domain of the molecule within the asymmetric unit (Fig. 5). Interestingly, F496 and V500, which are involved in SiRHP binding (Askenasy et al., 2018), are within 20 Å of the FMN cofactor from this symmetry partner. The third symmetry partner binds through charge-charge interactions between its connection domain and the FNR domain of the opposing molecule.

3.6. Effect of the ΔAAPSQS linker truncation on SiR/SiRFP-60-SiRHP dimer activity

We further characterized the impact of the ΔAAPSQS truncation on SiRFP function, as either full-length octamer or SiRFP-60 monomer. We purified the holoenzyme complex containing either WT SiRFP or SiRFP-ΔAAPSQS to homogeneity (Fig. S6A). The holoenzyme variants have overlapping UV–Vis spectra, showing that the truncation variant does not affect subunit-subunit binding or cofactor occupancy (Fig. S6B). The significant mass difference between the holoenzyme (800 kDa) and its subunits (the SiRFP octamer is 540 kDa and the SiRHP monomer is 64 kDa) allows isolation of stoichiometric complex via size exclusion chromatography (SEC) (Askenasy et al., 2015). WT SiR showed specific activity of 1500 ± 190 NADPH/min*siroheme, similar to the rate we measured for SiR-ΔAAPSQS of 1300 ± 30 NADPH/min*siroheme (Fig. 6A). Both activities agreed with specific activities of holoenzyme purified from source (Siegel et al., 1973).

We then independently purified SiRFP-60, SiRFP-60-ΔAAPSQS, and SiRHP. SDS-PAGE analysis of SiRP-60 and SiRFP-60-ΔAAPSQS (Fig. S6A) and UV–Vis spectroscopic analysis of SiRFP-60 and SiRFP-60-ΔAAPSQS show that the proteins are purified to homogeneity with good cofactor occupancy (Fig. S6B). The SiRFP-60/SiRHP dimer is 140 kDa, whereas each individual subunit is about 60 kDa, so there is significant overlap in SEC analysis from tightly-bound and free subunits. Therefore, we used a mixture of SiRHP with 2-fold excess SiRFP-60 or SiRFP-60-ΔAAPSQS to assess the impact of the internal truncation on SiRFP-60 function. Specific activities were calculated in terms of siroheme concentration because SiRHP was limiting in dimer formation (siroheme is SiRHP's heme-like cofactor (Murphy and Siegel, 1973)). The SiFRP-60/SiRHP mixture has a specific activity of 120 ± 7 NADPH/min*siroheme whereas the SiRFP-60-ΔAAPSQS/SiRHP mixture has a specific activity of 40 ± 2 NADPH/min*siroheme (Fig. 6B).

As a control, we tested whether electron transfer between SiRFP-60 and SiRHP occurred only between two tightly bound subunits or if electron transfer between pre-formed SiRFP-60-ΔAAPSQS/SiRHP dimer and free SiRFP-60 was possible. We generated the dimer SiRFP-60-ΔAAPSQS and SiRHP with a 2:1 ratio, as before. Then, we added 2.5-fold excess free SiRFP-60 that was active for electron transfer to SiRHP. Additional reductase does not significantly recover the specific activity of the reaction (Fig. 6B).

We also measured the ability of SiRFP-60 or SiRFP-60-ΔAAPSQS to reduce cytochrome *c*, which does not bind SiRFP-60 to form a stable complex, to test if the reduced activity of SiRFP-60-ΔAAPSQS was due to the nature of the interactions between SiRFP and SiRHP or a general defect in function. SiRFP-60 reduces cytochrome *c* with a specific activity of 2500 ± 190 heme/min*flavin but SiRFP-60-ΔAAPSQS reduces cytochrome *c* with a specific activity of 370 ± 35 heme/min*flavin (Fig. 6C).

We further wanted to assess if SiRFP-60-ΔAAPSQS's reduced activity was due to a defect in intra-molecular flavin electron transfer, so we chemically reduced SiRFP variants with NADPH or sodium dithionite in the absence of oxidase partner. Reduction of the flavins bleaches their characteristic 458 nm absorbance (Zeghouf et al., 1998) and for NADPH to reduce the flavins, the Fld domain must dock at the connection/FNR domain in the closed conformation so that the FAD and FMN cofactors make close contact (Figs. 2 and S1) (Hamdane et al., 2009). The analogous linker truncation in CPR inhibits the ability of NADPH to fully reduce its flavins (Hamdane et al., 2009). Dithionite reduction does not need the conformational change because it reduces the flavins directly. All SiRFP variants were reduced by both NADPH and sodium dithionite (Figs. 7 and S7).

4. Discussion

4.1. SiRFP is more extended than CPR

SiR is a multi-subunit oxidoreductase that funnels electrons from cellular NADPH pools to the SO_3^{2-} substrate through an octameric diflavin reductase, SiRFP. Homology between SiRFP and CPR predicts that SiRFP functions through a redox-dependant conformational change described in the cytochrome system. When CPR is oxidized, the Fld domain closes to bring the FMN cofactor close to the FAD cofactor. When NADPH binds, two electrons move onto the flavin cofactors and the reduced Fld domain swings open by about 15° to allow a transient interaction with a cytochrome oxidase that takes the electrons one-by-

UNCORRECTED PROOF

one from the FMN to the substrates, bound at the heme active site (Fig. 2A and B). Other chemistries catalyzed by similar oxidoreductases are one or two electron reductions (Haque et al., 2014). SiR catalyzes a six-electron reduction so each turnover consumes three NADPH equivalents (Fig. 1B).

In SiRFP, the Fld domain adopts an extended position relative to the connection-FNR domains allowed by the extended linker, more extreme than seen in CPR (Figs. 1A and 2). Importantly, solution scattering measured on SiRFP-60 and SiRFP-60-ΔAAPSQS reveals an R_g of about 30 Å for both, consistent with the extended position of the Fld domain and about 10 Å larger than the compact, closed form seen in oxidized CPR (Figs. 4 and S3). A symmetry partner recapitulates the CPR closed form, drawing the redox cofactors together from separate polypeptides (Figs. 5 and S4). The theoretical R_g calculation from this domain pairing is similar to that measured on oxidized CPR (Freeman et al., 2017) but does not agree with our SANS measurements (Fig. S3), suggesting this is not the primary conformation that SiRFP-60 or SiRFP-60-ΔAAPSQS adopts in solution.

4.2. Potential for inter-subunit reciprocity

Our crystal structure reveals three different structural relationships between the Fld and connection/FNR domains. First, the open conformation exposes to solution the FMN cofactor from which electrons move to SiRHP (Fig. 1C). Second, a symmetry-related molecule inserts its Fld domain into the large cavity allowed by the open Fld domain, mimicking the closed conformation seen in CPR (Figs. 5 and S4). Third, a symmetry-related Fld domain sits near the NADPH and the SiRHP binding sites at F496/V500 (Figs. 5 and S5). Siroheme-dependent sulfite reductase, whether dodecameric or dimeric, catalyzes a high-volume electron transfer that necessitates three productive SiRFP-SiRHP interactions per turnover event in the six-electron reduction of SO_3^{2-} to S^{2-} (Fig. 1B). Recapitulation of the closed, electron-transfer competent conformation in the crystal structure suggests that there could be flexibility in how SiRFP passes electrons. The NADPH-FAD from one FNR domain could reduce the Fld domain intra-molecularly from the same protein, as it does in CPR, or inter-molecularly, from a neighboring subunit, allowing electron transfer to SiRHP (Fig. 8). There is precedence for such intra-molecular electron transfer in NOS (Haque et al., 2012).

The implications of the extended Fld domain position on SiR function are threefold. First, SiRFP's Fld domain likely takes on a different position than CPR when passing off electrons to its oxidase partner. CPR binds heme oxidase and cytochrome *c* in the open cleft between the Fld and FNR domains (Freeman et al., 2018; Sugishima et al., 2014). Our biochemical analysis of SiR shows that SiRHP binds SiRFP on the other side of the FNR domain from this position (Askenasy et al., 2018, 2015), which means SiRFP must access alternative conformations for electron transfer to its partner. Second, SiRFP-60 exists in an extended conformation even when it is oxidized (Figs. 4 and S3). Perhaps SiRFP samples different Fld positions more readily than CPR, allowed because of the added flexibility afforded by the 30 amino acid linker found in SiRFP (Fig. 1A), significantly longer than the 12 amino acid linker in CPR. Alternatively, in the absence of its octameric partners, SiRFP-60 could be more conformationally dynamic than it is in the oligomer. Certainly, these possibilities are not mutually exclusive.

4.3. Electron transfer in an oligomeric oxidoreductase

The minimal dimer between SiRFP-60 and SiRHP is active for SO_3^{2-} reduction, albeit with reduced activity over SiR (compare Fig. 6A and B). Shortening the linker through the ΔAAPSQS truncation further reduces the activity of the dimer and additional, free SiRFP-60 does not rescue its activity (Fig. 6B). Similarly, shortening the linker reduces SiRFP-60's ability to reduce a non-endogenous, transiently-bound cytochrome *c* partner (Fig. 6C). In contrast, the internal ΔAAPSQS truncation does not affect the activity of the dodecameric SiR holoenzyme.

These observations could be explained by several non-exclusive possibilities. First, the ΔAAPSQS linker truncation could hinder SiRFP's ability to perform intra-molecular electron transfer by preventing the FMN from being reduced by the NADPH-reduced FAD. Second, the ΔAAPSQS linker truncation could hinder the conformational changes needed to pass the electrons to the SiRHP or cytochrome *c* oxidase partner. Third, the oligomeric nature of the dodecameric SiR holoenzyme could bypass either requirement. We directly tested the first by measuring whether the SiRFP variations in this study could be reduced by NADPH or sodium dithionite. Each variation was reduced, eliminating the first possibility and supporting the hypothesis that the long linker plays a role in repositioning the Fld domain for productive electron transfer to its oxidase partner.

One mystery that remains about SiR is how the Fld domain, once reduced, makes its way to SiRHP that is bound at the back side of the FNR domain (Askenasy et al., 2018, 2015). Our results suggest that in addition to performing the opening/closing that allows FAD-to-FMN electron transfer, the Fld domain performs electron transfer to a tightly bound SiRHP by repositioning to the interface formed by D182/R250, E196/H491, and R200/N251. The 30 amino acid linker, if extended, is long enough to make the ~50 Å-long trip around the connection/FNR domain if it were in an extended conformation. In monomeric SiRFP-60, this interaction must occur in *cis* because there is only one copy of each subunit. The conformational change from the closed conformation to the SiRHP-adjacent conformation must occur three times to pass all six electrons, in part explaining why the dimer has a lower specific activity than SiR holoenzyme (Fig. 6). In contrast, the dodecamer supplies a higher local concentration of Fld domains relative to SiRHP because of the $\alpha_8\beta_4$ stoichiometry.

5. Conclusions

Despite obvious similarities amongst various diflavin reductase homologs, we show in this study that the mechanism of inter-cofactor electron transfer differs in a homolog-specific way. Specifically, we report that SiRFP operates under a new paradigm, in which the oxidized form of the multidomain structure is in an extended conformation that places the Fld domain far from the FAD cofactor, joined by a long linker. Further, there are differential effects on dimeric or dodecameric forms of SiR from shortening the linker or altering amino acids that may help position the Fld domain for productive electron transfer. These observations suggest that in the dodecameric SiR holoenzyme electron transfer occurs via multiple pathways, bypassing the need for electrons to move intra-molecularly from the NADH to the FAD to the FMN and then in *cis* to SiRHP. In this way, SiR effectively raises the local concentration of electrons relative to SiRHP active sites to facilitate the full six electron reduction of SO_3^{2-} to S^{2-}.

Acknowledgements

A portion of this research at ORNL's Spallation Neutron Source was sponsored by the Scientific User Facilities Division, Office of Basic Energy Sciences, U.S. Department of Energy. The authors kindly thank Jen Kennedy and Dr. Christopher Stroupe for helpful discussions as well as Dr. Thayamanusamy Somasundaram and the Institute of Molecular Biophysics for support of the X-ray diffraction data collection.

Funding

This work was supported by National Science Foundation award MCB1149763 to MES and a GRFP to JMP.

UNCORRECTED PROOF

Author contributions

AMT performed the crystallographic experiments and refined the structure. IA performed the biochemical analysis of the SiRFP variants. JMP collected the X-ray data. DTM, CBS, and MES collected the SANS data. MES designed the study, oversaw the experimentation, processed the SANS data with help from CBS, and wrote the manuscript.

Declaration of interest

The authors declare there are no competing interests.

Appendix A. Supplementary data

Supplementary data to this article can be found online at https://doi.org/10.1016/j.jsb.2019.01.001.

References

Adams, P.D., Afonine, P.V., Bunkoczi, G., Chen, V.B., Davis, I.W., Echols, N., Headd, J.J., Hung, L.W., Kapral, G.J., Grosse-Kunstleve, R.W., McCoy, A.J., Moriarty, N.W., Oeffner, R., Read, R.J., Richardson, D.C., Richardson, J.S., Terwilliger, T.C., Zwart, P.H., 2010. PHENIX: a comprehensive Python-based system for macromolecular structure solution. Acta Crystallogr. D Biol. Crystallogr. 66, 213–221.

Aigrain, L., Pompon, D., Moréra, S., Truan, G., 2009. Structure of the open conformation of a functional chimeric NADPH cytochrome P450 reductase. EMBO Rep. 10, 742–747.

Arnold, O., Bilheux, J.C., Borreguero, J.M., Buts, A., Campbell, S.I., Chapon, L., Doucet, M., Draper, N., Ferraz Leal, R., Gigg, M.A., Lynch, V.E., Markvardsen, A., Mikkelson, D.J., Mikkelson, R.L., Miller, R., Palmen, K., Parker, P., Passos, G., Perring, T.G., Peterson, P.F., Ren, R., Reuter, M.A., Savici, A.T., Taylor, J.W., Taylor, R.J., Tolchenov, R., Zhou, W., Zikovsky, J., 2014. Mantid – data analysis and visualization package for neutron scattering and μ SR experiments. Nucl. Instruments Methods Phys. Res. Sect. A Accel. Spectrometers, Detect. Assoc. Equip. 764, 156–166.

Askenasy, I., Murray, D.T., Andrews, R.M., Uversky, V.N., He, H., Stroupe, M.E., 2018. Structure-function relationships in the oligomeric nadph-dependent assimilatory sulfite reductase. Biochemistry 57, 3764–3772.

Askenasy, I., Pennington, J.M., Tao, Y., Marshall, A.G., Young, N.L., Shang, W., Stroupe, M.E., 2015. The N-terminal domain of Escherichia coli assimilatory NADPH-sulfite reductase hemoprotein is an oligomerization domain that mediates holoenzyme assembly. J. Biol. Chem. 290, 19319–19333.

Barton, L.L., Ritz, N.L., Fauque, G.D., Lin, H.C., 2017. Sulfur cycling and the intestinal microbiome. Dig. Dis. Sci. 62, 2241–2257.

Crane, B.R., Getzoff, E.D., 1996. The relationship between structure and function for the sulfite reductases. Curr. Opin. Struct. Biol. 6, 744–756.

Emsley, P., Lohkamp, B., Scott, W.G., Cowtan, K., 2010. Features and development of Coot. Acta Crystallogr. D Biol. Crystallogr. 66, 486–501.

Eschenbrenner, M., Coves, J., Fontecave, M., 1995. NADPH-sulfite reductase flavoprotein from Escherichia coli: contribution to the flavin content and subunit interaction. FEBS Lett. 374, 82–84.

Eschenbrenner, M., Coves, J., Fontecave, M., 1995. The flavin reductase activity of the flavoprotein component of sulfite reductase from Escherichia coli. A new model for the protein structure. J. Biol. Chem. 270, 20550–20555.

Freeman, S.L., Martel, A., Raven, E.L., Roberts, G.C.K., 2017. Orchestrated domain movement in catalysis by cytochrome P450 reductase. Sci. Rep. 7, 9741.

Freeman, S.L., Martel, A., Devos, J.M., Basran, J., Raven, E.L., Roberts, G.C.K., 2018. Solution structure of the cytochrome P450 reductase-cytochrome. J. Biol. Chem. 293, 5210–5219.

Gruez, A., Pignol, D., Zeghouf, M., Coves, J., Fontecave, M., Ferrer, J.L., Fontecilla-Camps, J.C., 2000. Four crystal structures of the 60 kDa flavoprotein monomer of the sulfite reductase indicate a disordered flavodoxin-like module. J. Mol. Biol. 299, 199–212.

Hamdane, D., Xia, C., Im, S.C., Zhang, H., Kim, J.J., Waskell, L., 2009. Structure and function of an NADPH-cytochrome P450 oxidoreductase in an open conformation capable of reducing cytochrome P450. J. Biol. Chem. 284, 11374–11384.

Haque, M.M., Fadlalla, M.A., Aulak, K.S., Ghosh, A., Durra, D., Stuehr, D.J., 2012. Control of electron transfer and catalysis in neuronal nitric-oxide synthase (nNOS) by a hinge connecting its FMN and FAD-NADPH domains. J. Biol. Chem. 287, 30105–30116.

Haque, M.M., Bayachou, M., Tejero, J., Kenney, C.T., Pearl, N.M., Im, S.C., Waskell, L., Stuehr, D.J., 2014. Distinct conformational behaviors of four mammalian dual-flavin reductases (cytochrome P450 reductase, methionine synthase reductase, neuronal nitric oxide synthase, endothelial nitric oxide synthase) determine their unique catalytic profiles. FEBS J. 281, 5325–5340.

Hsieh, Y.C., Liu, M.Y., Wang, V.C., Chiang, Y.L., Liu, E.H., Wu, W.G., Chan, S.I., Chen, C.J., 2010. Structural insights into the enzyme catalysis from comparison of three forms of dissimilatory sulphite reductase from Desulfovibrio gigas. Mol. Microbiol. 78, 1101–1116.

Huang, C.W., Walker, M.E., Fedrizzi, B., Gardner, R.C., Jiranek, V., 2017. Hydrogen sulfide and its roles in Saccharomyces cerevisiae in a winemaking context. FEMS Yeast Res. 17.

Huang, W.C., Ellis, J., Moody, P.C., Raven, E.L., Roberts, G.C., 2013. Redox-linked domain movements in the catalytic cycle of cytochrome p450 reductase. Structure 21, 1581–1589.

Hubbard, P.A., Shen, A.L., Paschke, R., Kasper, C.B., Kim, J.J., 2001. NADPH-cytochrome P450 oxidoreductase. Structural basis for hydride and electron transfer. J. Biol. Chem. 276, 29163–29170.

Im, S.C., Waskell, L., 2011. The interaction of microsomal cytochrome P450 2B4 with its redox partners, cytochrome P450 reductase and cytochrome b(5). Arch. Biochem. Biophys. 507, 144–153.

Kasper, C.B., 1971. Biochemical distinctions between the nuclear and microsomal membranes from rat hepatocytes. J. Biol. Chem. 246, 577–581.

Konarev, P.V., Volkov, V.V., Sokolova, A.V., Koch, M.H.J., Svergun, D.I., 2003. PRIMUS: a Windows PC-based system for small-angle scattering data analysis. J. Appl. Cryst. 36, 1277–1282.

Laursen, T., Jensen, K., Moller, B.L., 2011. Conformational changes of the NADPH-dependent cytochrome P450 reductase in the course of electron transfer to cytochromes P450. Biochim. Biophys. Acta, Gene Struct. Expression 1814, 132–138.

Mirts, E.N., Petrik, I.D., Hosseinzadeh, P., Nilges, M.J., Lu, Y., 2018. A designed heme-[4Fe-4S] metalloenzyme catalyzes sulfite reduction like the native enzyme. Science 361, 1098–1101.

Murphy, M.J., Siegel, L.M., 1973. Siroheme and sirohydrochlorin. The basis for a new type of porphyrin-related prosthetic group common to both assimilatory and dissimilatory sulfite reductases. J. Biol. Chem. 248, 6911–6919.

Oliveira, T.F., Vonrhein, C., Matias, P.M., Venceslau, S.S., Pereira, I.A., Archer, M., 2008. The crystal structure of Desulfovibrio vulgaris dissimilatory sulfite reductase bound to DsrC provides novel insights into the mechanism of sulfate respiration. J. Biol. Chem. 283, 34141–34149.

Olteanu, H., Banerjee, R., 2001. Human methionine synthase reductase, a soluble P-450 reductase-like dual flavoprotein, is sufficient for NADPH-dependent methionine synthase activation. J. Biol. Chem. 276, 35558–35563.

Olteanu, H., Wolthers, K.R., Munro, A.W., Scrutton, N.S., Banerjee, R., 2004. Kinetic and thermodynamic characterization of the common polymorphic variants of human methionine synthase reductase. Biochemistry 43, 1988–1997.

Panda, K., Ghosh, S., Stuehr, D.J., 2001. Calmodulin activates intersubunit electron transfer in the neuronal nitric-oxide synthase dimer. J. Biol. Chem. 276, 23349–23356.

Panda, K., Rosenfeld, R.J., Ghosh, S., Meade, A.L., Getzoff, E.D., Stuehr, D.J., 2002. Distinct dimer interaction and regulation in nitric-oxide synthase types I, II, and III. J. Biol. Chem. 277, 31020–31030.

Parey, K., Warkentin, E., Kroneck, P.M., Ermler, U., 2010. Reaction cycle of the dissimilatory sulfite reductase from Archaeoglobus fulgidus. Biochemistry 49, 8912–8921.

Petoukhov, M.V., Franke, D., Shkumatov, A.V., Tria, G., Kikhney, A.G., Gajda, M., Gorba, C., Mertens, H.D., Konarev, P.V., Svergun, D.I., 2012. New developments in the program package for small-angle scattering data analysis. J. Appl. Crystallogr. 45, 342–350.

Pettersen, E.F., Goddard, T.D., Huang, C.C., Couch, G.S., Greenblatt, D.M., Meng, E.C., Ferrin, T.E., 2004. UCSF Chimera–a visualization system for exploratory research and analysis. J. Comput. Chem. 25, 1605–1612.

Schiffer, A., Parey, K., Warkentin, E., Diederichs, K., Huber, H., Stetter, K.O., Kroneck, P.M., Ermler, U., 2008. Structure of the dissimilatory sulfite reductase from the hyperthermophilic archaeon Archaeoglobus fulgidus. J. Mol. Biol. 379, 1063–1074.

Sibille, N., Blackledge, M., Brutscher, B., Coves, J., Bersch, B., 2005. Solution structure of the sulfite reductase flavodoxin-like domain from Escherichia coli. Biochemistry 44, 9086–9095.

Siddhanta, U., Wu, C., Abu-Soud, H.M., Zhang, J., Ghosh, D.K., Stuehr, D.J., 1996. Heme iron reduction and catalysis by a nitric oxide synthase heterodimer containing one reductase and two oxygenase domains. J. Biol. Chem. 271, 7309–7312.

Siddhanta, U., Presta, A., Fan, B., Wolan, D., Rousseau, D.L., Stuehr, D.J., 1998. Domain swapping in inducible nitric-oxide synthase. Electron transfer occurs between flavin and heme groups located on adjacent subunits in the dimer. J. Biol. Chem. 273, 18950–18958.

Siegel, L.M., Davis, P.S., 1974. Reduced nicotinamide adenine dinucleotide phosphate-sulfite reductase of enterobacteria. IV. The Escherichia coli hemoflavoprotein: subunit structure and dissociation into hemoprotein and flavoprotein components. J. Biol. Chem. 249, 1587–1598.

Siegel, L.M., Murphy, M.J., Kamin, H., 1973. Reduced nicotinamide adenine dinucleotide phosphate-sulfite reductase of enterobacteria. I. The Escherichia coli hemoflavoprotein: molecular parameters and prosthetic groups. J. Biol. Chem. 248, 251–264.

Singh, S.B., Lin, H.C., 2015. Hydrogen sulfide in physiology and diseases of the digestive tract. Microorganisms 3, 866–889.

Smith, K.W., Stroupe, M.E., 2012. Mutational analysis of sulfite reductase hemoprotein reveals the mechanism for coordinated electron and proton transfer. Biochemistry 51, 9857–9868.

Sugishima, M., Sato, H., Higashimoto, Y., Harada, J., Wada, K., Fukuyama, K., Noguchi, M., 2014. Structural basis for the electron transfer from an open form of NADPH-cytochrome P450 oxidoreductase to heme oxygenase. Proc. Natl. Acad. Sci. U S A 111, 2524–2529.

Svergun, D.I., 1992. Determination of the regularization parameter in indirect-transform methods using perceptual criteria. J. Appl. Crystallogr. 25, 495–503.

UNCORRECTED PROOF

Svergun, D.I., 1999. Restoring low resolution structure of biological macromolecules from solution scattering using simulated annealing. Biophys. J. 76, 2879–2886.

Svergun, D.I., Richard, S., Koch, M.H., Sayers, Z., Kuprin, S., Zaccai, G., 1998. Protein hydration in solution: experimental observation by X-ray and neutron scattering. Proc. Natl. Acad. Sci. U S A 95, 2267–2272.

Townsend, G.T., Ramanand, K., Suflita, J.M., 1997. Reductive dehalogenation and mineralization of 3-chlorobenzoate in the presence of sulfate by microorganisms from a methanogenic aquifer. Appl. Environ. Microbiol. 63, 2785–2791.

Wang, M., Roberts, D.L., Paschke, R., Shea, T.M., Masters, B.S., Kim, J.J., 1997. Three-dimensional structure of NADPH-cytochrome P450 reductase: prototype for FMN- and FAD-containing enzymes. Proc. Natl. Acad. Sci. U S A 94, 8411–8416.

Wasmund, K., Mußmann, M., Loy, A., 2017. The life sulfuric: microbial ecology of sulfur cycling in marine sediments. Environ. Microbiol. Rep. 9, 323–344.

Wignell, G.D., Bates, F.S., 1987. Absolute calibration of small-angle neutron scattering data. J. Appl. Crystallogr. 20, 28–40.

Wolthers, K.R., Scrutton, N.S., 2007. Protein interactions in the human methionine synthase-methionine synthase reductase complex and implications for the mechanism of enzyme reactivation. Biochemistry 46, 6696–6709.

Wolthers, K.R., Basran, J., Munro, A.W., Scrutton, N.S., 2003. Molecular dissection of human methionine synthase reductase: determination of the flavin redox potentials in full-length enzyme and isolated flavin-binding domains. Biochemistry 42, 3911–3920.

Wolthers, K.R., Toogood, H.S., Jowitt, T.A., Marshall, K.R., Leys, D., Scrutton, N.S., 2007. Crystal structure and solution characterization of the activation domain of human methionine synthase. FEBS J. 274, 738–750.

Wu, J.Y., Siegel, L.M., Kredich, N.M., 1991. High-level expression of Escherichia coli NADPH-sulfite reductase: requirement for a cloned cysG plasmid to overcome limiting siroheme cofactor. J. Bacteriol. 173, 325–333.

Xia, C., Hamdane, D., Shen, A.L., Choi, V., Kasper, C.B., Pearl, N.M., Zhang, H., Im, S.C., Waskell, L., Kim, J.J., 2011. Conformational changes of NADPH-cytochrome P450 oxidoreductase are essential for catalysis and cofactor binding. J. Biol. Chem. 286, 16246–16260.

Yokom, A.L., Morishima, Y., Lau, M., Su, M., Glukhova, A., Osawa, Y., Southworth, D.R., 2014. Architecture of the nitric-oxide synthase holoenzyme reveals large conformational changes and a calmodulin-driven release of the FMN domain. J. Biol. Chem. 289, 16855–16865.

Zeghouf, M., Fontecave, M., Coves, J., 2000. A simplified functional version of the Escherichia coli sulfite reductase. J. Biol. Chem. 275, 37651–37656.

Zeghouf, M., Fontecave, M., Macherel, D., Coves, J., 1998. The flavoprotein component of the Escherichia coli sulfite reductase: expression, purification, and spectral and catalytic properties of a monomeric form containing both the flavin adenine dinucleotide and the flavin mononucleotide cofactors. Biochemistry 37, 6114–6123.

Zhang, H., Yokom, A.L., Cheng, S., Su, M., Hollenberg, P.F., Southworth, D.R., Osawa, Y., 2018. The full-length cytochrome P450 enzyme CYP102A1 dimerizes at its reductase domains and has flexible heme domains for efficient catalysis. J. Biol. Chem. 293, 7727–7736.

Zhao, J.K., Gao, C.Y., Liu, D., 2010. The extended Q -range small-angle neutron scattering diffractometer at the SNS. J. Appl. Crystallogr. 43, 1068–1077.

UNCORRECTED PROOF